LBNL-43946
Preprint

ERNEST ORLANDO LAWRENCE
BERKELEY NATIONAL LABORATORY

Molecular Thermodynamics of Precipitation

Francesco Fornasiero, Jan Ulrich,
and John M. Prausnitz

Chemical Sciences Division

July 1999

Submitted to
Chemical Engineering and Processing

REFERENCE COPY
Does Not
Circulate
Bldg. 50 Library - Ref.
Lawrence Berkeley National Laboratory

Copy 1

LBNL-43946

DISCLAIMER

This document was prepared as an account of work sponsored by the United States Government. While this document is believed to contain correct information, neither the United States Government nor any agency thereof, nor the Regents of the University of California, nor any of their employees, makes any warranty, express or implied, or assumes any legal responsibility for the accuracy, completeness, or usefulness of any information, apparatus, product, or process disclosed, or represents that its use would not infringe privately owned rights. Reference herein to any specific commercial product, process, or service by its trade name, trademark, manufacturer, or otherwise, does not necessarily constitute or imply its endorsement, recommendation, or favoring by the United States Government or any agency thereof, or the Regents of the University of California. The views and opinions of authors expressed herein do not necessarily state or reflect those of the United States Government or any agency thereof or the Regents of the University of California.

LBNL-43946

Molecular thermodynamics of precipitation

Francesco Fornasiero, Jan Ulrich and John M. Prausnitz
Department of Chemical Engineering
University of California
and
Chemical Sciences Division
Lawrence Berkeley National Laboratory
University of California
Berkeley, CA 94720, U.S.A.

July 1999

This work was supported by the Director, Office of Science, Office of Basic Energy Sciences Chemical Sciences Division of the U.S. Department of Energy under Contract Number DE-AC03-76SF00098.

Molecular thermodynamics of precipitation*

Francesco Fornasiero[a], Jan Ulrich[a, 1] and J. M. Prausnitz[a, 2]

[a] Chemical Engineering Department, University of California, Berkeley

and

Chemical Sciences Division, Lawrence Berkeley National Laboratory

Berkeley, CA 94720, USA

Abstract

Using a simple theory for fluids and a simple theory for a solid, it is possible to construct a semi-quantitative corresponding-states phase diagram where a reduced temperature is plotted as a function of a reduced density. The reducing parameters are molecular size (σ^3) and molecular potential energy (ε/k_B); the phase diagram includes both low-density and high-density fluid regions and the solid region. These calculations apply to a pure substance or, of more interest, to a solute dissolved in a continuous solvent. The qualitative nature of the phase diagram depends strongly on the range of attractive intermolecular forces as indicated by an exponential parameter n; when coordination number z=8 and n is about 6, we obtain the usual phase diagram where the fluid-solid region lies to the right of the fluid-fluid coexistence curve. But when n is about 7 or 8, the fluid-solid region lies above the fluid-fluid coexistence curve. Applications are discussed for aqueous solutions of a colloid or a globular protein that may also contain a salt or a polymer to induce precipitation.

Keywords: Van der Waals theory; Phase diagram; Protein precipitation.

---

* Dedicated to Professor E. U. Schlünder for his 70th birthday

[1] Present address: Automatic Control Laboratory, Swiss Federal Institute of Technology, ETH-Z, ETL I 22, CH-8092 Zurich, Switzerland

[2] Corresponding author. Fax: +01 510 642 4778, e-mail: prausnit@cchem.berkeley.edu

1. Introduction

In chemical engineering, precipitation provides a common method for the separation of fluid mixtures. For example, to separate sugar from its aqueous solution, it is necessary to increase the sugar concentration above its saturation value. We can do so by cooling or by evaporation of water. At saturation, we reach the phase boundary where the solvent is saturated and no longer able to "hold on" to any more solute. Alternatively, precipitation may be achieved at constant temperature and constant solute/solvent ratio by changing the nature of the solvent through addition of another substance, e.g. a polymer or a salt or a soluble gas or some liquid anti-solvent. In all these cases, precipitation occurs by changing conditions until the solution is at its saturation condition, i.e. at a phase boundary.

Thermodynamics provides a method for calculating phase boundaries. For a substance *i*, the boundary between phases ' and " is determined by the well-known relations:

$$T' = T''$$
$$p' = p''$$
$$\mu_i' = \mu_i''$$

where T and p stand for temperature and pressure and μ is the chemical potential. Molecular thermodynamics provides a method for calculating p and μ (at a given T and density ρ) from molecular properties. This method requires information on intermolecular forces and a theory of matter as expressed by statistical mechanics.

In this work, for simple substances, we present a statistical-thermodynamic method for calculating a phase diagram, i.e. a plot of temperature versus density. This plot shows phase boundaries, in particular the fluid-fluid boundary and the fluid-solid boundary. While details differ, our method is not original; in essence, it is based on recent research well documented in the physico-chemical literature

For our calculation, we require a theory for the fluid state (that is, for gases and liquids) and a theory for the solid state. Further, we require an expression for the

intermolecular potential function φ that provides quantitative information on intermolecular forces.

Because our purpose here is illustrative, we do not attempt to obtain quantitative agreement between a calculated and an observed phase diagram. For our purposes here, a semiquantitative result is sufficient. Therefore, to avoid excessively long and complex calculations, we use very simple models for the fluid phase, for the solid state and for φ.

From the derivation outlined below, we obtain a corresponding-states phase diagram where the reducing parameter for the temperature is ε/k and that for the density is σ^3; these parameters appear in φ. The interesting result of our derivation is that the qualitative nature of the phase diagram depends on the range of attractive intermolecular forces. On a plot of reduced temperature versus reduced density, for "normal" substances (e.g. argon or methane), the light-fluid/dense-fluid (vapor-liquid) coexistence curve lies to the left of the dense-fluid/solid coexistence region. However, for large particles (e.g. colloids or globular proteins) dissolved in a liquid, where particle-particle attractive forces extend over only a short range, the fluid-solid coexistence region lies above the light-fluid/dense-fluid coexistence curve. This theoretical result can provide guidance in the design of a precipitation process. After outlining our method for calculating the phase diagram, we discuss some examples of engineering interest.

2. Theoretical framework

We use molecular van der Waals models to describe both the fluid phase and the solid phase. In both cases, we apply a first-order perturbation theory for the Helmholtz energy of a hard-sphere reference system.

To calculate the fluid-solid coexistence curves, two models are required: one for the fluid phase and another for the solid phase. Each model provides an equation of state, one for the fluid (gas or liquid) and another for the solid.

The simplest non-trivial potential function is the inverse-power potential, used here to derive the perturbation terms for both equations of state:

$$\varphi(r)=\begin{cases}\infty & r<\sigma \\ -\varepsilon\left(\dfrac{\sigma}{r}\right)^n & r\geq\sigma \qquad (n>3)\end{cases} \tag{2.1}$$

where r is the center-to-center distance between the particles, σ is the hard-sphere diameter, and ε is the energy of maximum attraction. The hard-sphere reference systems are, respectively:

1. Carnahan-Starling [1] equation of state for the fluid phase;
2. Free-distance approximation for the compressibility factor of the solid phase [2].

In our discussion we use dimensionless equations because of their convenience for calculations. The dimensionless variables are defined as follows:

$$\tilde{A}=\frac{A}{N\cdot k_B\cdot T} \qquad \text{Helmholtz energy} \tag{2.2}$$

$$\tilde{\mu}=\frac{\mu}{k_B\cdot T} \qquad \text{chemical potential} \tag{2.3}$$

$$\tilde{T}=\frac{k_B\cdot T}{\varepsilon} \qquad \text{temperature} \tag{2.4}$$

$$\tilde{p}=\frac{p}{\rho_0\cdot\varepsilon} \qquad \text{pressure} \tag{2.5}$$

$$\tilde{r}=\frac{r}{\sigma} \qquad \text{center - to - center distance between two particles} \tag{2.6}$$

where

$$\rho_0=\frac{6}{\pi\cdot\sigma^3} \qquad \text{one - particle density (reciprocal volume of one particle)} \tag{2.7}$$

Here N is the number of particles in the system, k_B is the Boltzmann constant and ρ is the number density.

2.1. Van der Waals model for the fluid phase.

The Helmholtz energy for the fluid phase is the sum of two parts:

$$\tilde{A}=\tilde{A}^{ref}+\tilde{A}^{pert} \tag{2.8}$$

where

$$\tilde{A}^{ref} = \tilde{A}^{HS} = \ln\left(\rho\Lambda^3\right) - 1 + \int_0^{\eta}\left(Z^{HS} - 1\right)\frac{d\eta}{\eta} \tag{2.9}$$

$$\tilde{A}^{pert} = \frac{\rho \cdot \sigma^3}{2 \cdot \varepsilon \cdot \tilde{T}} \cdot \int_0^{\infty} \varphi(\tilde{r}) \cdot 4 \cdot \pi \cdot \tilde{r}^2 \cdot d\tilde{r} \tag{2.10}$$

Here Λ represents the thermal de Broglie wavelength, Z^{HS} is the compressibility factor of the hard-sphere system and η is the packing fraction defined by ρ/ρ_0. Subscript ref stands for reference and subscript pert stands for perturbation.

Equations (2.8)-(2.10) are based on three assumptions. These assumptions are characteristic of molecular van der Waals theory:

1. Starting from the Gibbs-Bogoliubov inequality, the upper bound of the Helmholtz energy is taken as the estimate of the Helmholtz energy of the system.
2. All correlations between molecules in the domain of the attractive potential are neglected. This assumption is the random-phase approximation (RPA).
3. The reference system is given by a hard-sphere system whose potential is:

$$\phi^{HS}(\tilde{r}) = \begin{cases} \infty & \tilde{r} \le 1 \\ 0 & \tilde{r} > 1 \end{cases} \tag{2.11}$$

The compressibility factor of the hard-sphere reference system for the fluid-phase is given by the Carnahan-Starling equation of state:

$$Z^{HS} = \frac{1 + \eta + \eta^2 - \eta^3}{(1-\eta)^3} \tag{2.12}$$

Substituting (2.1) and (2.12) into (2.9) and (2.10), respectively, yields for (2.8):

$$\tilde{A} = \ln\left(\rho_0\Lambda^3\right) - 1 + \ln(\eta) + \frac{4\eta - 3\eta^2}{(1-\eta)^2} - \frac{\eta}{\tilde{T}} \cdot \frac{12}{n-3} \tag{2.13}$$

Using standard thermodynamics, from $\tilde{A}$ we obtain the reduced pressure $\tilde{p}$ and the reduced chemical potential $\tilde{\mu}$:

$$\tilde{p} = \tilde{T} \cdot \eta^2 \cdot \left(\frac{\partial \tilde{A}}{\partial \eta}\right)_{\tilde{T},N} \tag{2.14}$$

$$\tilde{\mu} = \tilde{A} + \frac{\tilde{p}}{\eta \cdot \tilde{T}} \tag{2.15}$$

From (2.14), the pressure for the fluid phase is:

$$\tilde{p} = \tilde{T} \cdot \eta \cdot \frac{1+\eta+\eta^2-\eta^3}{(1-\eta)^3} - \eta^2 \cdot \frac{12}{n-3} \tag{2.16}$$

From (2.15), the chemical potential for the fluid phase is:

$$\tilde{\mu} = \ln(\rho_0 \Lambda^3) - 1 + \ln(\eta) + \frac{4\eta - 3\eta^2}{(1-\eta)^2} + \frac{1+\eta+\eta^2-\eta^3}{(1-\eta)^3} - 2 \cdot \frac{\eta}{\tilde{T}} \cdot \frac{12}{n-3} \tag{2.17}$$

2.2. Van der Waals model for the solid phase.

To obtain an expression for the Helmholtz energy of the solid phase, we use a derivation similar to that for the fluid phase. The Helmholtz énergy for the solid phase is obtained from Equation (2.8); however, the reference term and the perturbation term are now calculated using models appropriate for a solid.

For the equation of state of a hard-sphere solid, we use a free-distance approximation that leads to a very simple expression of the compressibility factor:

$$Z^{HS} = \frac{1}{1 - d^{\frac{1}{3}}} \tag{2.18}$$

where d is defined by

$$d = \frac{\rho}{\rho_{cp}} = \frac{\eta}{\eta_{cp}} \tag{2.19}$$

In (2.19), η_{cp} is the close-packed packing fraction whose value depends on the assumed structure of the solid phase; for example, for a face-centered cubic lattice with coordination number z=12, we have $\eta_{cp} = 0.74048$, while for a body-centered cubic lattice with z=8, we have $\eta_{cp} = 0.68$.

As d→0, Z^{HS} of the solid phase goes to unity, i.e. to an ideal gas. Therefore, it is possible to integrate Equation (2.9) yielding the reference term of the Helmholtz energy for the solid phase:

$$\tilde{A}^{ref} = \ln(\rho_0 \Lambda^3) - 1 + \ln(\eta) - 3\ln\left(1 - d^{\frac{1}{3}}\right) \tag{2.20}$$

where $d^{\frac{1}{3}}$ is the reduced nearest-neighbor distance between two particles in the solid state.

For the perturbation term, we follow the model of Daanoun et al. [2] that represents the solid phase as a perfect crystal wherein the intermolecular center-to-center separation is determined by d and the density profile is given by a delta function on lattice sites. In this model, the perturbation term for the Helmholtz energy is proportional to the product of lattice coordination number z and the pair potential evaluated at the system's intermolecular separation $\widetilde{R} = d^{-\frac{1}{3}}$; as shown in Appendix I, the Helmoltz energy for the solid is

$$\widetilde{A} = \ln\left(\rho_0 \Lambda^3\right) - 1 + \ln(\eta) - 3\ln\left(1 - \frac{1}{\widetilde{R}}\right) - \frac{z}{2 \cdot \widetilde{T}} \cdot \frac{1}{\widetilde{R}^n} \tag{2.21}$$

The pressure and the chemical potential for the solid state follow directly from Equations (2.14) and (2.15):

$$\widetilde{p} = \widetilde{T} \cdot \eta \cdot \frac{1}{1 - \frac{1}{\widetilde{R}}} - \eta \cdot \frac{z \cdot n}{6} \cdot \frac{1}{\widetilde{R}^n} \tag{2.22}$$

$$\widetilde{\mu} = \ln\left(\rho_0 \Lambda^3\right) - 1 + \ln(\eta) - 3\ln\left(1 - \frac{1}{\widetilde{R}}\right) - \frac{z}{2 \cdot \widetilde{T}} \cdot \frac{1}{\widetilde{R}^n} + \frac{1}{1 - \frac{1}{\widetilde{R}}} - \frac{z \cdot n}{6 \cdot \widetilde{T}} \cdot \frac{1}{\widetilde{R}^n} \tag{2.23}$$

For both models, fluid and solid, the compressibility factor goes to unity as the density goes to zero; therefore, the chemical potential of the solid phase and the fluid phase refer to the same ideal-gas standard state. The compressibility factor for the fluid phase Z_F is

$$Z_F = \frac{\widetilde{p}}{\widetilde{T} \cdot \eta} = \frac{1 + \eta + \eta^2 - \eta^3}{(1 - \eta)^3} - \frac{\eta}{\widetilde{T}} \cdot \frac{12}{n - 3} \tag{2.24}$$

and the compressibility factor for the solid phase Z_S is

$$Z_S = \frac{\widetilde{p}}{\widetilde{T} \cdot \eta} = \frac{1}{1 - \frac{1}{\widetilde{R}}} - \frac{1}{\widetilde{T}} \cdot \frac{z \cdot n}{6} \cdot \frac{1}{\widetilde{R}^n} \tag{2.25}$$

As $\rho \to 0$, $\eta \to 0$ and $\widetilde{R} \to \infty$; thus the first term on the right side of Equation (2.24) and that of Equation (2.25) are equal to unity. The second terms are equal to zero, provided $n > 3$.

3. Procedure for computing phase equilibria

The fluid-fluid coexistence curve and fluid-solid coexistence curve are calculated by solving simultaneously the equations:

$$\begin{cases} \tilde{p}'(\tilde{T},\eta') = \tilde{p}''(\tilde{T},\eta'') \\ \tilde{\mu}'(\tilde{T},\eta') = \tilde{\mu}''(\tilde{T},\eta'') \end{cases} \tag{3.1}$$

The symbols ′ and ″ refer to any pair of phases at equilibrium, either a fluid-fluid or a solid-fluid pair.

Equations (3.1) contain three variables; to obtain a solution, one of these variables has to be fixed. We choose the packing fraction (density) of the dilute fluid phase and then solve for the equilibrium temperature and for the packing fraction of the dense phase (dense fluid or solid).

3.1. Fluid-fluid equilibrium

The fluid-fluid coexistence curve is obtained by inserting expressions for the pressure and the chemical potential for the fluid phase, Equations (2.16) and (2.17), in both sides of Equations (3.1).

Equations (3.1), with pressure and chemical potential given by Equations (2.16) and (2.17), lead to a law of corresponding states, that gives a universal coexistence curve $(\tilde{T}/\tilde{T}_c \; vs. \; \eta/\eta_c)$, independent of parameter n in the inverse power potential. Here $\tilde{T}_c$=1.132/(n-3) and η_c=0.13044. Details are given in Appendix II.

3.2. Solid-fluid equilibrium

Calculation of the solid-fluid equilibrium curve requires again solution of the two-phase coexistence Equations (3.1), but now the mathematical expression for the right side is not the same as that for the left side. The pressure and the chemical potential are given by Equations (2.16) and (2.17) for the fluid phase, and by Equations (2.22) and (2.23) for the solid phase.

To perform phase-equilibrium calculations with different models for the two phases, it is necessary that careful attention is given to standard states. For the equations presented here, the standard state for each of the phases is the ideal gas at system temperature and density. However, sometimes different standard states are used. In that event, it is necessary to inter-relate them by other information (See, for example, reference [3])

3.3. Triple point

Solution of the equations for fluid-fluid equilibrium and solution of those for the solid-fluid equilibrium does not tell us which phases are stable at a given temperature.

To determine what phases are physically present and to construct the correct phase diagram, it is necessary to calculate the triple point. In a one-component, argon-like system, starting the calculation with a very low density of the dilute fluid, we establish the solid-dilute fluid coexistence curve until we reach the triple temperature T_t where two fluid phases coexist with the solid, that is, where the freezing line (also called the liquidus line[3]) intersects the fluid-fluid coexistence curve. We then continue the diagram with the solid-dense fluid and fluid-fluid coexistence curve for temperatures above the triple temperature.

To determine the triple point, we solve simultaneously four equations that combine the fluid-fluid and the solid-fluid equilibrium conditions:

$$\begin{cases} \tilde{p}_f\left(\tilde{T},\eta_{f1}\right)=\tilde{p}_f\left(\tilde{T},\eta_{f2}\right) \\ \tilde{p}_s\left(\tilde{T},\eta_s\right)=\tilde{p}_f\left(\tilde{T},\eta_{f1}\right) \\ \tilde{\mu}_f\left(\tilde{T},\eta_{f1}\right)=\tilde{\mu}_f\left(\tilde{T},\eta_{f2}\right) \\ \tilde{\mu}_s\left(\tilde{T},\eta_s\right)=\tilde{\mu}_f\left(\tilde{T},\eta_{f1}\right) \end{cases} \tag{3.2}$$

There, subscript f1 refers to one fluid phase and subscript f2 to the other. Because a one-component system at its triple point has zero degrees of freedom (as given by the phase-rule), we do not fix any variable; there is only one unique solution to Equation (3.2).

[3] The liquidus line indicates the coordinates (temperature and density) where precipitation of solid is incipient.

Some systems, like colloids or fullerene C_{60}, do not show a triple point. Instead, these system show a fluid-fluid coexistence curve that lies below the liquidus line, i.e. the dense fluid phase is unstable or metastable. The relative positions of the phase boundaries are related to the interaction range between the particles and the coordination number for the solid phase [3,4] as briefly discussed later.

The switching point between the two shapes of phase diagram is given by the condition $T_c=T_t$; when $T_c>T_t$, the dense fluid phase is stable. Asherie et al. [4] proposed a measure of the metastability of the dense fluid phase; this measure is given by the "metastability gap":

$$g = \frac{T_s - T_c}{T_c} \tag{3.3}$$

where T_s is the temperature of the liquidus line at the critical density. When $g<0$, we have an argon-like phase diagram but when $g>0$, we have a colloid-like phase diagram. In the latter case, to calculate the phase diagram, we use the same procedure as that described above for solid-fluid equilibrium.

Appendix II shows that, for any expression for Z^{HS}, the reduced critical temperature depends only on ψ defined by

$$\Psi = \frac{12}{\varepsilon} \cdot \int_0^\infty \varphi(\tilde{r}) \cdot \tilde{r}^2 \cdot d\tilde{r} \tag{3.4}$$

For the inverse power potential,

$$\Psi = -\frac{12}{n-3} \tag{3.4a}$$

As discussed in Appendix II, Equation (3.4a) indicates that the dimensionless critical temperature declines as n increases.

Because a high value of n corresponds to a short-range attractive interaction while a low value corresponds to a long-range attractive interaction, the metastability gap g increases as the range of attraction falls. This increase leads to a shift from an argon-like to a colloid-like phase diagram.

Strong interactions (large ε) between the particles lead to a high critical temperature. At constant temperature, an increase in ε brings a decrease in $\tilde{T}$. By changing the nature of

the solvent such that ε rises, precipitation can be induced without changing the temperature.

3.4. Critical point

To obtain the vapor-liquid or liquid-liquid critical point of the fluid-fluid coexistence curve we solve two equations:

$$\begin{cases} \left(\dfrac{\partial \tilde{p}}{\partial \eta}\right)_{\tilde{T},N} = 0 \\ \left(\dfrac{\partial^2 \tilde{p}}{\partial \eta^2}\right)_{\tilde{T},N} = 0 \end{cases} \tag{3.5}$$

As a consequence of van der Waals theory, the packing fraction at the critical point is a constant that depends only on the hard-sphere reference system, as shown in Appendix II.

4. Results and discussion

We first discuss how the phase diagram changes with the range of attractive forces; we then present two applications to aqueous protein solutions using salt or polymer as precipitating agent.

4.1. Effect of the range of attractive forces

As pointed out by numerous authors in recent years [2,4-8], the range of the attractive part of the intermolecular potential determines the qualitative shape of the phase diagram, i.e. whether or not a given system has a stable dense fluid phase.

In our model the range of attractive intermolecular forces is determined by exponent n of the inverse power potential given by Equation (2.1). As shown in Figure 1, the range of attractive interaction declines with increasing n.

Figure 2.a indicates how n affects the qualitative features of the phase diagram. For z=8, a relatively low value of n (~6) gives the usual type of phase diagram with a fluid-fluid critical point and a triple line. Upon increasing n, i.e. shortening the range of attractive forces, the triple line moves toward the fluid-fluid critical point touching it at

n=7.46. Appendix II shows that, for our model, the fluid-fluid coexistence curve follows a law of corresponding states, independent of n and z.

If the range of attraction is further shortened, only two stable phases remain: the light (or dilute) fluid phase and the solid phase. For n=8, the fluid-fluid coexistence curve lies underneath the liquidus line. In other words, the fluid-solid phase equilibrium leads to a global minimum of the free energy, while the fluid-fluid equilibrium corresponds to a local minimum [8]. Thus, when z=8, the metastability gap g defined by Equation (3.3) is negative for n<7.46, equal to zero for n=7.46 and positive for n>7.46.

Figure 2.b is similar to Figure 2.a but now z=12. We notice that the qualitative features of the phase boundaries do not change: as n increases, the liquidus line shifts to the left side of the fluid-fluid coexistence curve, leading to a transition of the phase diagram from an argon-type to a colloid-type phase diagram. However, for z=12, the range of attractive forces necessary to stabilize the dense fluid phase is longer (lower n) than that for z=8, in agreement with Asherie's results [4]. For z=12, the transition value is n=5.8.

4.2. Aqueous solution of globular proteins

An inexpensive and common method for precipitating proteins from aqueous solution is achieved by adding salt or a nonionic polymer as precipitating agent [9]. Also, protein crystallization is a necessary preliminary step for determining the three-dimensional structures of proteins by x-ray diffraction. Growing a suitable protein crystal is not simple, because solubility and crystallization are governed by many factors, including temperature, pH, ionic strength, protein size and charge distribution as well as the nature and concentration of added precipitating agents [10-12].

A generalized (that is, reduced) protein-solution phase diagram may be useful for design of a protein-separation process.

To illustrate, we consider here two cases: precipitation of lysozyme by adding salt, and polymer-induced precipitation of human serum albumin, both from aqueous solutions.

For both illustrations, we use the one-fluid assumption, i.e. we describe the solution as a pseudo one-component system where the biomacromolecular solute is dissolved in a mixed solvent [13]. The potential function for describing particle-particle forces in a medium is now the potential of mean force. The same assumption has been introduced by other authors using somewhat different models for aqueous one-protein solutions [6] or for aqueous protein mixtures [3,14].

The packing fraction η is related to the protein mass concentration c by:

$$\eta = \frac{\pi \cdot \sigma^3}{6} \cdot \frac{N_A}{M_w} \cdot c \tag{4.1}$$

where N_A is Avogadro's number and M_w is the protein molecular weight. The light fluid in the phase diagram is the dilute uniform protein solution, the fluid-fluid coexistence curve is the liquid-liquid binodal and the liquidus line is the protein's solubility curve. The pressure is the osmotic pressure of the protein solution.

Figure 3.a shows the calculated solubility curve and the liquid-liquid coexistence curve for hen egg-white lysozyme solutions with 3, 5, 7% w/v NaCl at pH=4.5 in the temperature range 4 to 25 °C. Experimental data are also shown. Calculations were performed with η_c=0.13044 and T_c=297.3, 315.2 and 324.7 K, respectively, for 3, 5, 7% w/v NaCl solutions. Solubility data are from [15]; experimental cloud points are from [16].

Liquid-liquid phase separation occurs underneath the liquidus line, i.e. it is metastable with respect to the solid-liquid transition. There is growing evidence that the features of the lysozyme phase diagram are typical for solutions of globular proteins [12]. Similar behavior has been observed for many native variants of γ-crystallin [17-20]. The presence of a hidden metastable fluid-fluid binodal inside the fluid-crystal region has been related to the often observed formation of amorphous precipitates in crystallization processes and to an increase of the rate of crystal nucleation [8,16,21].

As discussed by several authors and confirmed by Monte Carlo simulation [5], if the range of interaction between colloidal particles is sufficiently short, experiment often shows liquid-liquid coexistence that is metastable with respect to solidification. To generate a phase diagram where the fluid-fluid coexistence curve lies below the liquidus line, it is necessary that the attractive range be short. The transition is obtained when the

size of the attraction range lies between 0.15 and 0.3 times the size of the colloidal particle [2,4,5,7].

For solutions of globular protein solutions, the essential features of the phase diagram can be understood by considering that proteins in such solutions often have short-range attractive interactions, especially when the solution conditions are close to saturation [22,23]. The addition of salt as precipitating agent screens electrostatic repulsion between the particles and enhances protein-protein attractive forces. At high salt concentrations, precipitation of protein is enhanced by an osmotic free-volume effect as discussed elsewhere [24]. For most salts, as salt concentration rises, protein solubility falls.

Figure 3.a shows both calculated and experimental results. For the calculation, z, n and σ were fixed respectively at 8, 8.2 and 34.4 A [25] and only ε (i.e. T_c) was used as adjustable parameter. Agreement with experimental solubility data is fairly good; however, the description of the metastable liquid-liquid separation is only qualitative, due to the simplicity of our model; as is well known, a mean-field theory cannot give good results in the critical region.

The regressed T_c increases with salt concentration reflecting higher attractive protein-protein interactions. The calculated T_c values have been compared with those regressed from experimental data for the osmotic second virial coefficient obtained at similar conditions [26]. The relation between interaction potential and second virial coefficient is given by:

$$B_{22} = 2\pi\sigma^3 \int_{\sigma}^{\infty} \left[1 - e^{-\varphi(\bar{r})/k_B T}\right] \cdot r^2 dr = \frac{2\pi\sigma^3}{3}\left[1 - \frac{3}{n-3}\left(\frac{\varepsilon}{k_B T}\right)\right] = \frac{2\pi\sigma^3}{3}\left[1 - 3\alpha\frac{T_c}{T}\right] \qquad (4.2)$$

where α is a constant equal to 0.8834.

The approximation introduced in Equation (4.2) is consistent with the simplicity of our model [3]. When solubility data are used to obtain T_c and when independent second-osmotic-virial-coefficient data are also used to obtain T_c (from Equation (4.2)), fairly good agreement is obtained, as indicated in Figure 4.

Figure 3.b shows a comparison between experiment and calculation for z=12 and n=6.3. The accuracy of the calculation is comparable to that in Figure 3.a. The regressed

T_c and the calculated second virial coefficient for z=12 are very close to those obtained for z=8.

Another example, given in Figure 5, shows the effect of increasing polyethylene glycol (PEG) concentration in an aqueous solution of human serum albumin (HSA) at protein concentration 45.7 g/L. Experimental data are from Atha and Ingham [27] at 22-24 °C in 0.05M potassium acetate buffer, pH=4.5, containing 0.1M KCl. PEG is a water-soluble, nonadsorbing, nontoxic polymer widely used in the chemical and biochemical industries. It allows regulation of protein solubility without any effect on protein structure and function [27-29]. The polymer appears to interact with the dissolved proteins merely by an excluded-volume effect: the magnitude of interaction is primarily controlled by the polymer concentration; polymer molecular weight is less important.

George and Wilson [11] have shown that proteins tend to form crystals only when the solvent is moderately poor, i.e. for slightly negative second virial coefficients B_{22}. In a good solvent (positive B_{22}), there is no precipitation, and in a very poor solvent (large negative B_{22}), precipitation gives an amorphous structure. Therefore, too much additive (either salt or polymer) tends to give an amorphous precipitate. George and Wilson [11] have determined a narrow, well-defined range of B_{22} [-1×10^{-4} to -8×10^{-4} mol ml/ g^2] where protein crystallization is likely to occur.

Regression of the reducing parameter T_c at different PEG concentrations shows an enhancement of attractive interaction between the protein particles as we increase the PEG concentration in the protein solution (see Figure 6). Thus, starting with a solution at protein concentration of 45.7 g/L in absence of added polymer and then increasing the PEG4000 concentration, the point representing the solution at given temperature and protein concentration moves vertically down from the one fluid-phase region toward the fluid-solid boundary. At polymer concentration 8% (w/v), the solubility curve is reached; the corresponding value of T_c is 265.9 K when z=8, n=8 and σ=70.4 A (σ is from the hydrodynamic radius reported by Atha and Ingham, [27]).

To compare our result with George and Wilson's work [11], we use the expression for the second virial coefficient given by Equation (4.2): the calculated B_{22} value falls inside the crystallization slot. Following Rosenbaum et al. [12], we can define a crystallization slot in terms of dimensionless variable T/T_c, independent of z, n and σ.

Rewriting Equation (4.2) for the second virial coefficient in dimensionless form, and equating it with Rosembaum's second virial coefficient calculated with an adhesive hard-sphere potential, we obtain:

$$\frac{B_{22}^{IP}}{B_{22}^{HS}} = 1 - 3\alpha\frac{T_c}{T} = \frac{B_{22}^{AHS}}{B_{22}^{HS}} = 1 - \frac{1}{4\tau} \tag{4.3}$$

where the hard-sphere second virial coefficient is given by

$$B_{22}^{HS} = \frac{2\pi\sigma^3}{3} \tag{4.4}$$

and τ is the effective reduced temperature for the adhesive hard-sphere potential. Superscripts IP and AHS stand for inverse power and adhesive hard-sphere, respectively.

For the adhesive hard-sphere potential, the crystallization slot is approximately given by $0.06<\tau<0.15$. Converting τ to T/T_c by (4.3), for our model we obtain the crystallization slot $0.636<T/T_c<1.59$.

At higher polymer concentration (>8%), the point representing our solution falls inside the two-phase fluid-solid region. Our model predicts that, for a PEG concentration equal to 13.1%, the fluid-fluid coexistence curve is reached. Even if we do not have experimental verification of the quantitative prediction, the qualitative result is nevertheless interesting considering the explanation given by Poon [8] of the cessation of crystallization at high additive concentration. He suggested that "the non-crystallization boundary should be identified with a metastable gas-liquid[4] binodal buried in the equilibrium fluid-crystal coexistence region". When a system has a short-range intermolecular attraction, inhibited phase transition kinetics may lead to a metastable amorphous precipitate. The regressed T_c corresponding to 13.1% PEG concentration gives a second virial coefficient that is inside the crystallization slot. However, Curtis' work [26] shows that the condition defined by George and Wilson [11] is probably necessary but not sufficient for crystallization. Even if the protein-protein second virial coefficient lies inside the crystallization slot, amorphous precipitate can appear, because as the reduced temperature falls, transition to a crystal may be "missed" due to the requirement that crystals can form only when the crystallizing molecules have the proper orientation.

[4] Here "gas" refers to dilute solution.

If the reduced temperature falls too quickly, the protein molecules may be inhibited from forming a crystal when the liquidus line is reached. Further reduction in the reduced temperature may then lead to precipitation of a second fluid phase where orientation requirements are much lower than those for formation of a crystal.

5. Conclusion

Using simple van der Waals theories to model the fluid phase and the solid phase, it is possible to reproduce the phase behavior either of argon-like systems or of colloid-like systems. In the former case, the phase diagram gives a triple point and the light-fluid/dense-fluid coexistence curve lies to the left of the dense fluid/solid coexistence region on a plot of temperature versus density; in the latter case, there is no triple point because the light-fluid/dense-fluid coexistence curve lies underneath the liquidus line.

In a dimensionless phase diagram, where a reduced temperature T/T_c is plotted as a function of a reduced density η/η_c, our model shows that a decrease in the range of attractive forces between the particles leads to a shift of the liquidus line to the left of the fluid-fluid coexistence curve. For sufficiently short range attraction ($n>7.46$ when $z=8$), the latter is buried inside the fluid/solid coexistence region and the triple point disappears. For such systems, while the fluid/solid equilibrium corresponds to a global minimum of the free energy, the fluid-fluid equilibrium corresponds to a local minimum of the free energy; therefore, fluid-fluid equilibria are not thermodynamically stable.

Two applications are discussed for aqueous protein solutions, using salt or polymer to induce precipitation. In the first example, NaCl is added as precipitating agent to aqueous lysozyme solutions. Despite the simplicity of the model, semi-quantitative agreement is obtained between lysozyme-solubility experimental data and the calculated liquidus line at different NaCl concentration. The regressed critical temperature increases as the sodium chloride concentration in solution rises, in accord with enhancement of the attractive protein-protein interaction due to the salt screening effect of the electrostatic repulsion between the particles and, at high salt concentration, due to an osmotic free-volume effect. However, description of the liquid-liquid coexistence curve is only qualitative.

The second example presents the effect of increasing polyethylene glycol concentration in aqueous solution of human serum albumin. The addition of polyethylene glycol to a protein solution leads to an increase of the attractive interaction between the particles by an osmotic excluded-volume effect. For some relatively high polymer concentration, the protein solid-liquid boundary can be reached and crystallization can be induced. The interesting result of our calculation is the prediction of fluid-fluid separation at high polymer concentration, even if it is metastable with respect to the thermodynamically stable fluid-solid transition. This prediction is due to the strict requirement of a proper orientation of the crystallizing molecules to give a crystal. When the liquidus line is reached rapidly, poor solvent conditions (large negative second virial coefficient) can inhibit the protein molecules from forming the ordered (crystal) solid phase. In that event, addition of polymer can induce the kinetically favored separation of a second fluid phase where orientation requirements are much lower.

Acknowledgment

For financial support, the authors are grateful to the Director, Office of Science, Office of Basic Energy Sciences, U.S. Department of Energy. J. Ulrich acknowledges with thanks support from a Solvay fellowship, F. Fornasiero support from the Rotary International Club. All authors express their gratitude to Robin Curtis for helpful advice.

Appendix I: Helmholtz energy for the solid phase

The Helmoltz energy for the solid phase is given by the sum of two terms, the Helmholtz energy of the hard-sphere reference system and the perturbation Helmholtz energy:

$$\tilde{A} = \tilde{A}^{ref} + \tilde{A}^{pert} \tag{I.1}$$

where

$$\tilde{A}^{ref} = \tilde{A}^{HS} = \ln\left(\rho\Lambda^3\right) - 1 + \int_0^{\eta} \left(Z^{HS} - 1\right)\frac{d\eta}{\eta} \tag{I.2}$$

$$\tilde{A}^{pert} = \frac{1}{2 \cdot \varepsilon \cdot \tilde{T}} \cdot \int_0^{\infty} \varphi(\tilde{r}) \cdot \rho(\tilde{r}) \cdot 4 \cdot \pi \cdot \tilde{r}^2 \cdot d\tilde{r} \tag{I.3}$$

As shown in Section 1.2, the reference term is given by

$$\tilde{A}^{ref} = \ln(\rho_0 \Lambda^3) - 1 + \ln(\eta) - 3\ln\left(1 - d^{\frac{1}{3}}\right) \tag{I.4}$$

To calculate the perturbation energy, we follow Daanoun et al. [2]. The density profile is approximated by delta functions on the lattice sites $\tilde{r}_j$:

$$\rho(\tilde{r}) = \sum_{j=1}^{sites} \delta(\tilde{r} - \tilde{r}_j) \tag{I.5}$$

where δ is the dirac delta function. Inserting Equation (I.5) into Equation (I.3), we obtain:

$$\tilde{A}^{pert} = -\frac{1}{2 \cdot \varepsilon \cdot \tilde{T}} \sum_{j=1}^{sites} \varphi(\tilde{r}_j) \tag{I.6}$$

Rewriting Equation (2.23) in terms of a sum over spherical shells of sites centered around the site at the origin, we obtain

$$\tilde{A}^{pert} = -\frac{1}{2 \cdot \varepsilon \cdot \tilde{T}} \sum_{j=1}^{shells} n_j \cdot \varphi(\tilde{r}_j) \tag{I.7}$$

where n_j is the number of sites of the jth shell. For a potential function $\varphi(\tilde{r})$ that decreases rapidly as $\tilde{r}$ rises, we need only the dominant term as a good approximation for the perturbation term:

$$\tilde{A}^{pert} = -\frac{z}{2 \cdot \varepsilon \cdot \tilde{T}} \cdot \varphi(\tilde{R}) \tag{I.8}$$

From Equation (I.1) we have the complete expression for the Helmholtz energy for the solid phase:

$$\tilde{A} = \ln(\rho_0 \Lambda^3) - 1 + \ln(\eta) - 3\ln\left(1 - \frac{1}{\tilde{R}}\right) - \frac{z}{2 \cdot \tilde{T}} \cdot \frac{1}{\tilde{R}^n} \tag{I.9}$$

Appendix II:
Corresponding states for the fluid-fluid coexistence curve

As a consequence of the first-order perturbation theory and the random-phase approximation (RPA), fluid-fluid equilibria follow a law of corresponding states.

We demonstrate that Equations (3.1) for fluid-fluid equilibria can be rewritten as functions only of η/η_c and T/T_c.

First we show that the packing fraction at the critical point is a constant depending only on the hard-sphere reference system and that the critical temperature is proportional to 1/(n-3).

First, we rewrite the expression of the pressure in the more general form:

$$\tilde{p} = \tilde{T} \cdot \eta \cdot Z^{HS} + \eta^2 \cdot \Psi \tag{II.1}$$

where

$$\Psi = \frac{12}{\varepsilon} \cdot \int_0^\infty \varphi(\tilde{r}) \cdot \tilde{r}^2 \cdot d\tilde{r} \tag{II.2}$$

and we calculate the critical point using Equations (3.5):

$$\begin{cases} \left(\dfrac{\partial \tilde{p}}{\partial \eta}\right)_{\tilde{T},N} = \tilde{T} \cdot \left(Z^{HS} + \eta \cdot \left(\dfrac{\partial Z^{HS}}{\partial \eta}\right)\right) + 2 \cdot \eta \cdot \Psi = 0 \\ \left(\dfrac{\partial^2 \tilde{p}}{\partial \eta^2}\right)_{\tilde{T},N} = \tilde{T} \cdot \left(2 \cdot \left(\dfrac{\partial Z^{HS}}{\partial \eta}\right) + \eta \cdot \left(\dfrac{\partial^2 Z^{HS}}{\partial \eta^2}\right)\right) + 2 \cdot \Psi = 0 \end{cases} \tag{II.3}$$

The last equation can be solved for $\tilde{T}$:

$$\tilde{T} = -\frac{2 \cdot \Psi}{\left(2 \cdot \left(\dfrac{\partial Z^{HS}}{\partial \eta}\right) + \eta \cdot \left(\dfrac{\partial^2 Z^{HS}}{\partial \eta^2}\right)\right)} \tag{II.4}$$

Substituting Equation (II.4) into the first of Equations (II.3), we obtain the relation:

$$\frac{Z^{HS} + \eta \cdot \left(\dfrac{\partial Z^{HS}}{\partial \eta}\right)}{\left(2 \cdot \left(\dfrac{\partial Z^{HS}}{\partial \eta}\right) + \eta \cdot \left(\dfrac{\partial^2 Z^{HS}}{\partial \eta^2}\right)\right)} - \eta = 0 \tag{II.5}$$

that depends only on the hard-sphere compressibility factor.

The critical packing fraction η_c is given by solution of Equation (II.5). For the Carnahan-Starling hard-sphere compressibility factor, it is 0.13044.

Having shown that the critical packing fraction η_c is a constant for a given hard-sphere reference system, the critical density $\rho_c = \eta_c \cdot \frac{6}{\pi \cdot \sigma^3}$ increases as the particle diameter decreases in accord with experimental results.

In Equation (II.4), the denominator of the term in the right side, calculated at $\eta = \eta_c$, is a constant independent of n and z because the hard-sphere compressibility factor and its derivatives are functions only of the packing fraction η and because η_c is independent of n and z . As a consequence, the dimensionless critical temperature depends only on ψ. Inserting the inverse-power potential in Equation (II.2), we have

$$\Psi = -\frac{12}{n-3} \tag{II.6}$$

The critical temperature is thus proportional to 1/(n-3).

Second, we rewrite the chemical potential of the fluid phase in a more general form:

$$\tilde{\mu} = \ln(\rho_0 \Lambda^3) - 1 + \ln(\eta) + \int_0^{\eta} (Z^{HS} - 1)\frac{d\eta}{\eta} + Z^{HS} + 2 \cdot \frac{\eta}{\tilde{T}} \cdot \Psi \tag{II.7}$$

We then impose the equilibrium conditions, Equations (3.1):

$$\begin{cases} \tilde{T} \cdot \eta_1 \cdot Z^{HS}(\eta_1) + \eta_1^2 \cdot \Psi = \tilde{T} \cdot \eta_2 \cdot Z^{HS}(\eta_2) + \eta_2^2 \cdot \Psi \\ \ln(\eta_1) + \int_0^{\eta_1} (Z^{HS}(\eta) - 1)\frac{d\eta}{\eta} + Z^{HS}(\eta_1) + 2 \cdot \frac{\eta_1}{\tilde{T}} \cdot \Psi = \ln(\eta_2) + \int_0^{\eta_2} (Z^{HS}(\eta) - 1)\frac{d\eta}{\eta} + Z^{HS}(\eta_2) + 2 \cdot \frac{\eta_2}{\tilde{T}} \cdot \Psi \end{cases} \tag{II.8}$$

Equations (II.4)-(II.5) can be rewritten in compact form as follows:

$$\eta_c = c_1 \tag{II.9}$$

$$\Psi = c_2 \cdot \tilde{T}_c \tag{II.10}$$

where c_1 and c_2 are constants. Dividing the first Equation (II.8) by $\tilde{T}$ and inserting Equations (II.9) and (II.10) in Equation (II.8), where the packing fraction η is replaced by $(\eta/\eta_c) \cdot \eta_c$, we obtain equilibrium conditions containing only the reduced variables η/η_c and T/T_c, as desired:

$$\begin{cases} c_1 \cdot c_2 \cdot \dfrac{\eta_1}{\eta_c} \cdot Z^{HS}\left(\dfrac{\eta_1}{\eta_c}\right) + c_2 \cdot \left(c_1 \cdot \dfrac{\eta_1}{\eta_c}\right)^2 \cdot \dfrac{\tilde{T}_c}{\tilde{T}} = c_1 \cdot c_2 \cdot \dfrac{\eta_2}{\eta_c} \cdot Z^{HS}\left(\dfrac{\eta_2}{\eta_c}\right) + \left(c_1 \cdot \dfrac{\eta_2}{\eta_c}\right)^2 \cdot \dfrac{\tilde{T}_c}{\tilde{T}} \\ \ln\left(\dfrac{\eta_1}{\eta_c}\right) + \displaystyle\int_0^{\frac{\eta_1}{\eta_c}} \left(Z^{HS}\left(\dfrac{\eta}{\eta_c}\right) - 1\right) \dfrac{d\eta}{\eta} + Z^{HS}\left(\dfrac{\eta_1}{\eta_c}\right) + 2 \cdot c_1 \cdot c_2 \cdot \dfrac{\tilde{T}_c}{\tilde{T}} \cdot \left(\dfrac{\eta_1}{\eta_c} - \dfrac{\eta_2}{\eta_c}\right) - \ln\left(\dfrac{\eta_2}{\eta_c}\right) - \displaystyle\int_0^{\frac{\eta_2}{\eta_c}} \left(Z^{HS}\left(\dfrac{\eta}{\eta_c}\right) - 1\right) \dfrac{d\eta}{\eta} - Z^{HS}\left(\dfrac{\eta_2}{\eta_c}\right) = 0 \end{cases}$$

While the fluid-fluid equilibrium curve is independent of the range of attractive potential, the solid-fluid coexistence curve is not. There is no law of corresponding states for solid-fluid equilibrium.

Nomenclature

A	Helmholtz energy
B_{22}	second-virial-coefficient
c_1, c_2	constants
d	defined by Equation (2.19)
g	metastability gap
k_B	Boltzmann constant
M_w	molecular weight
n	exponent of the inverse power potential
N	number of particles
N_A	Avogadro's number
p	pressure
r	center to center distance between two particles
$\tilde{R}$	intermolecular separation for the solid phase
T	temperature
z	coordination number
Z	compressibility factor

Greek letters

α	constant

δ	dirac delta function
ε	energy of maximum attraction
η	packing fraction
Λ	de Broglie thermal wavelength
μ	chemical potential
ρ	number density
ρ_0	one-particle density
σ	hard-sphere diameter
τ	effective reduced temperature for the adhesive hard-sphere potential
φ	intermolecular potential function
Ψ	defined by Equation (3.4)

Subscripts

1	light fluid
2	dense fluid
c	critical
cp	closed packing
f, f1, f2	fluid
s	solid
t	triple point

Superscripts

′, ″	phases at equilibrium
~	dimensionless variables
AHS	adhesive hard-sphere
HS	hard-sphere
IP	inverse power
pert	perturbation
ref	reference

References

[1] Carnahan N., and K. Starling, "Equation of State for Nonattracting Rigid Spheres", *J. Chem. Phys.*, **51**, 635 (1970).

[2] Daanoun A., C. F. Tejero, and M. Baus, "Van der Waals Theory for Solids", *Phys. Rev. E.*, **50**, 2913 (1994).

[3] Hino T., and J. M. Prausnitz, "Solid-Liquid Equilibria for Solutions of Binary Globular-Protein Mixtures", in press *AIChE J* (1999).

[4] Asherie N., A. Lomakin, and G. B. Benedek, "Phase Diagram of Colloidal Solutions", *Phys. Rev. Lett.*, **77**, 4832 (1996).

[5] Hagen M. H. J., and D. Frenkel, "Determination of Phase Diagram for the Hard-core Attractive Yukawa System", *J. Chem. Phys.*, **101**, 4093 (1994).

[6] Mahadevan H., and C. K. Hall, "Theory of Precipitation of Protein Mixtures by Nonionic Polymer", *AIChE J.*, **38**, 573 (1990).

[7] Ilett S. M., A. Orrock, W. C. K. Poon, and P. N. Pusey, "Phase Behavior of a Model Colloid-Polymer Mixture", *Phys. Rev. E.*, **51**, 1344 (1995).

[8] Poon W. C. K., "Crystallization of Globular Proteins", *Phys. Rev. E.*, **55**, 3762 (1997).

[9] Rothstein F., Differential Precipitation of Proteins", *Protein Purification Process Engineering*, R. G. Harrison, ed., Marcel Dekker, New York, (1994).

[10] McPherson A., *Preparation and Analysis of Protein Crystals*, Wiley, New York (1982)

[11] George A, and W. W. Wilson, "Predicting Protein Crystallization from a Dilute Solution Property", *Acta Cryst. D*, **50**, 361 (1994).

[12] Rosenbaum D., P. C. Zamora, and C. F. Zukoski, "Phase Behavior of Small Colloidal Attractive Particles", *Phys. Rev. Lett.*, **76**, 150 (1996).

[13] McMillan W. G., and J. E. Mayer, "The Statistical Thermodynamics of Multicomponent Systems", *J. Chem. Phys.*, **13**, 276 (1945).

[14] Mahadevan H., and C. K. Hall, "Statistical –Mechanical Model of Protein Precipitation by Nonionic Polymer", *AIChE J.*, **36**, 1517 (1992).

[15] Cacioppo E., and M. L. Pusey, "The Solubility of the Tetragonal Form of Hen Egg White Lysozyme from pH 4.0 to 5.4", *J. Crystal Growth*, **114**, 286 (1991).

[16] Muschol M., and Rosenberger F., "Liquid-liquid Phase Separation in Supersaturated Lysozyme Solutions and Associated Precipitate Formation/Crystallization", *J. Chem. Phys.*, **107**, 1953 (1997).

[17] Thomson J. A., P. Schutenberger G. M. Thurston, and G. B. Benedek, "Binary Liquid Phase Separation and Critical Phenomena in a Protein/Water Solution", *Proc. Natl. Acad. Sci. USA*, **84**, 7079 (1987).

[18] Schutenberger P., R. A. Chamberlin, G. M. Thurston, J. A.Thomson, and G. B. Benedek, "Observation of Critical Phenomena in a Protein-Water Solution", *Phys. Rev. Lett.*, **63**, 2064 (1989).

[19] Berland C. R., G. M. Thurston, M. Kondo, M. L. Broide, J. Pande, O. Ogun, and G. B. Benedek, "Solid-Liquid Phase Boundaries of Lens Protein Solution", *Proc. Natl. Acad. Sci. USA*, **89**,1214 (1992).

[20] Broide M. L., C. R.Berland, J. Pande, O. Ogun, and G. B. Benedek, "Binary-Liquid Phase Boundaries of Lens Protein Solution", *Proc. Natl. Acad. Sci. USA*, **88**,5660 (1991).

[21] Wolde P. R., and Frenkel D., "Enhancement of Protein Crystal Nucleation by Critical Density Fluctuations", *Science*, **77**, 1975 (1997).

[22] Lomakin A., N. Asherie, and G. B. Benedek, "Monte Carlo Study of Phase Separation in Aqueous Protein Solution", *J. Chem. Phys.*, **104**, 1646 (1996).

[23] Malfois M., F. Bonnete`, L. Belloni, and A. Tardieu, "A model of attractive Interactions to Account for Fluid-Fluid Phase Separation of Protein Solutions", *J. Chem. Phys.*, **105**, 3290 (1996).

[24] Chiew Y. C., D. E. Kuehner, H. W. Blanch, and J. M. Prausnitz, "Molecular Thermodynamics of Salt-induced Protein Precipitation", *AIChE J.*, **41**, 2150 (1995)

[26] Curtis R. A., "Protein-Protein and Protein-Salt Interactions in Concentrated Aqueous Electrolyte Solutions", M.S. thesis, Univ. of California, Berkeley (1996).

[25] Ulrich J. A., "Measurements of Aqueous Protein Interactions from Low-Angle Laser-Light Scattering and Molecular Thermodynamics of Salt-induced Protein Precipitation", Diplomarbeit, Univ. of Karlsruhe and Univ. of California, Berkeley (1997).

[27] Atha D.H., and K. C. Ingham, "Mechanism of Precipitation of Proteins by Polyethylene Glycols", *J. Biol. Chem.*, **256**, 12108 (1981).

[28] Haire R. N., W. A. Tisel, J. G. White, and A. Rosenberg, "On the Precipitation of Polymers: the Hemoglobin-Polyethylene Glycol System", *Biopolymers*, **23**, 2761 (1984).

[29] Hasko F., R. Vaszileva, and L. Halasz, "Solubility of Plasma Proteins in the Presence of Polyethylene Glycol", *Boitechnol. & Bioeng.*, **24**, 1931 (1982).

Figure captions

Figure 1. Inverse power potential with different exponent n. As n rises, the range of attractive interaction decreases.

Figure 2. Theoretical dimensionless phase diagram changes with the range of attractive interaction: (a) z=8 and η_{cp}=0.68 (b) z=12 and η_{cp}=0.74048. For both (a) and (b), $\tilde{T}_c$=1.132/(n-3) and η_c=0.13044.

Figure 3. Phase diagram for aqueous solutions of hen egg-white lysozyme with 3, 5, 7% w/v NaCl at pH=4.5 in the temperature range 4 to 25 °C. The open diamonds are solubility data from Cacioppo and Pusey (1991); the solid diamonds are cloud-point data from Muschol and Rosenberger (1997). The solid curves are theoretical fluid-solid and fluid-fluid coexistence curves calculated with (a) z=8 and n=8.2; (b) z=12 and n=6.3.

Figure 4: Comparison between critical temperatures regressed from lysozyme-solubility data (Cacioppo and Pusey, 1991) and those regressed from lysozyme second-virial-coefficient data (Curtis, 1996). Experimental conditions:

1. Solubility data: sodium chloride solutions with 100-mM sodium acetate buffer at pH=4.5 and temperature range 4 to 25 °C.
2. Second-virial-coefficient data: sodium chloride solutions with 50-mM sodium acetate buffer at pH=4.5 and T=25 °C

Figure 5. Polymer-induced precipitation of human serum albumin (HSA) in aqueous solution of HSA at protein concentration equal to 45.7 g/L using polyethylene glycol (PEG) 4000. Experimental data are from Atha and Ingham (1981). The open circles represent the conditions where the solution reaches (a) the solubility curve; (b) the liquid-liquid coexistence curve. The solid lines are the fluid-solid boundary and fluid-fluid

coexistence curve in the dimensionless diagram calculated with z=8 and n=8. Here F and S indicate fluid and solid regions, respectively.

Figure 6. Effect of polyethylene glycol (PEG) 4000 concentration in aqueous solution of human serum albumin (HSA) on T_c. Experimental data are from Atha and Ingham (1981).

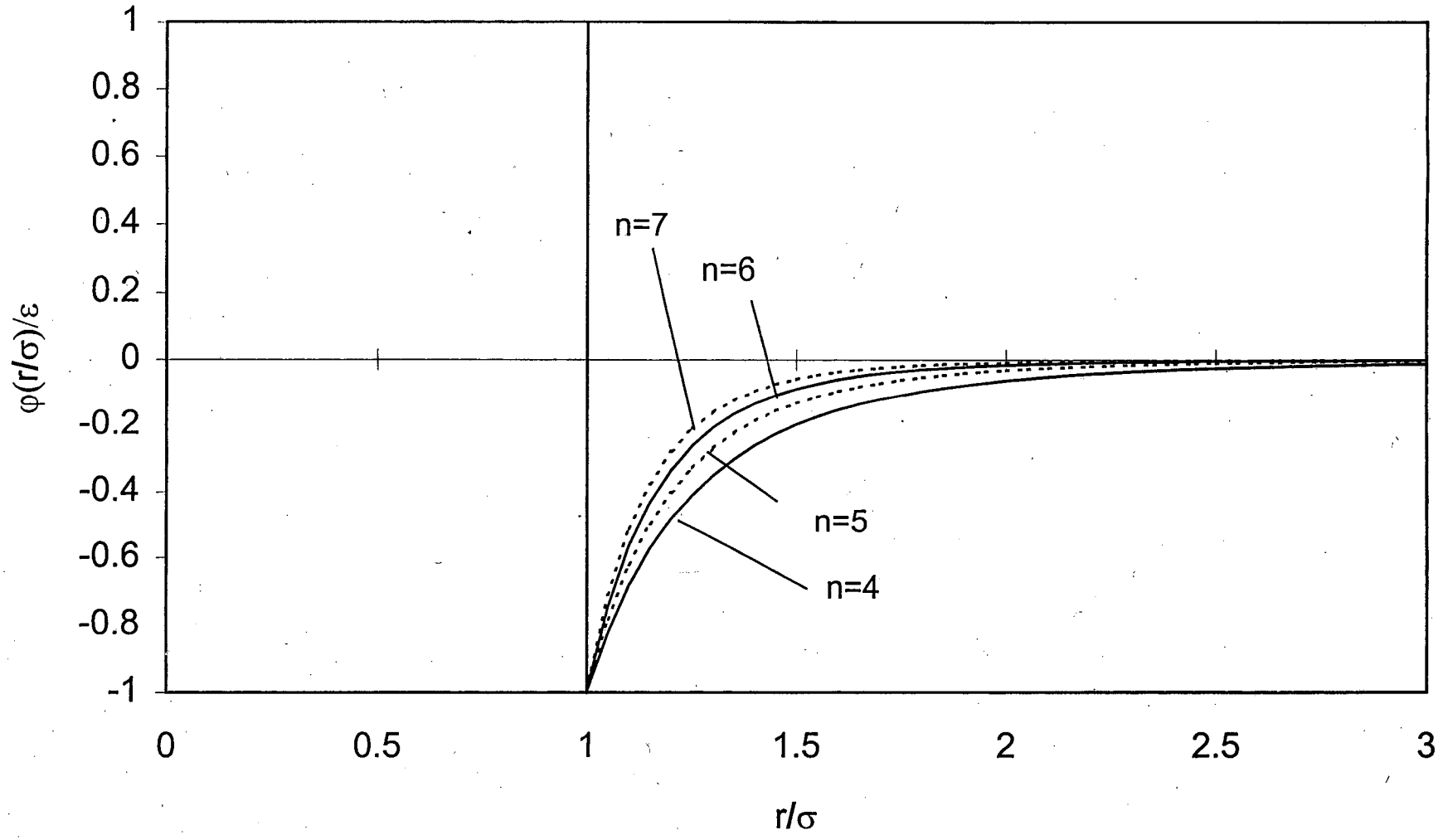

Figure 1

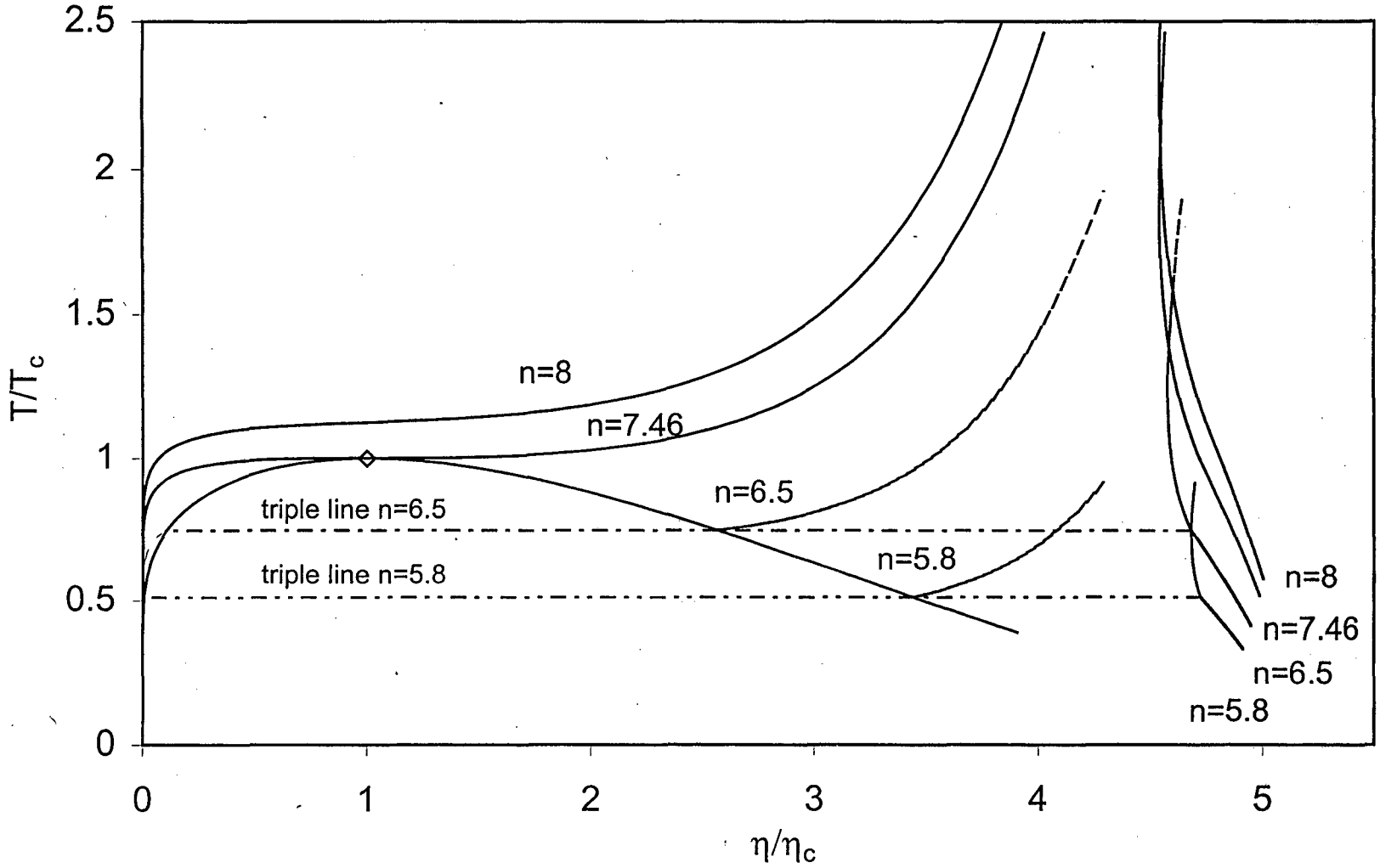
2.5
2
1.5
1
0.5
0
T/T_c
0
1
2
3
4
5
η/η_c
n=8
n=7.46
n=6.5
n=5.8
triple line n=6.5
triple line n=5.8
n=8
n=7.46
n=6.5
n=5.8

Figure 2.a

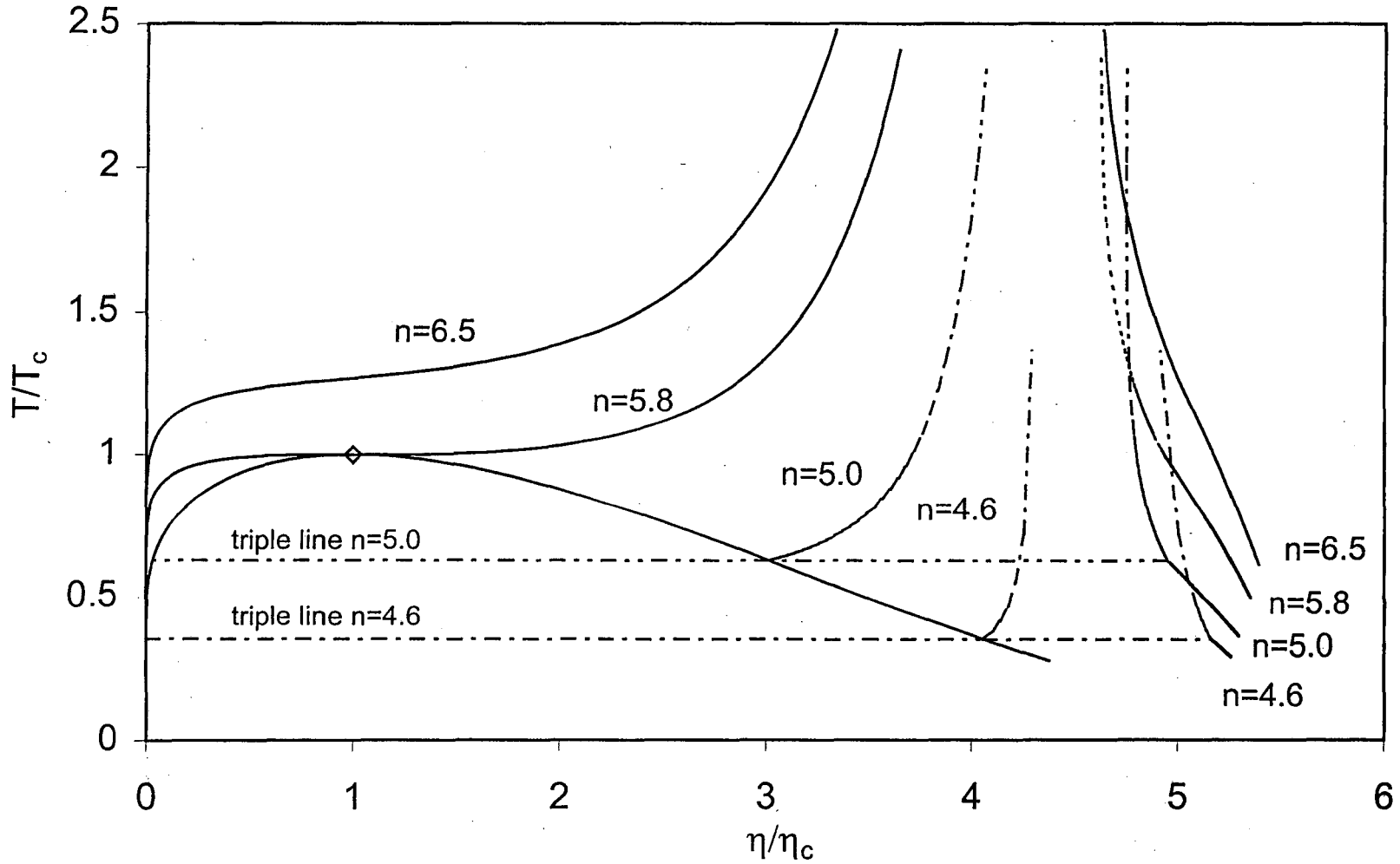
2.5
2
1.5
1
0.5
0
T/T_c
0
1
2
3
4
5
6
η/η_c
n=6.5
n=5.8
n=5.0
n=4.6
triple line n=5.0
triple line n=4.6
n=6.5
n=5.8
n=5.0
n=4.6

Figure 2.b

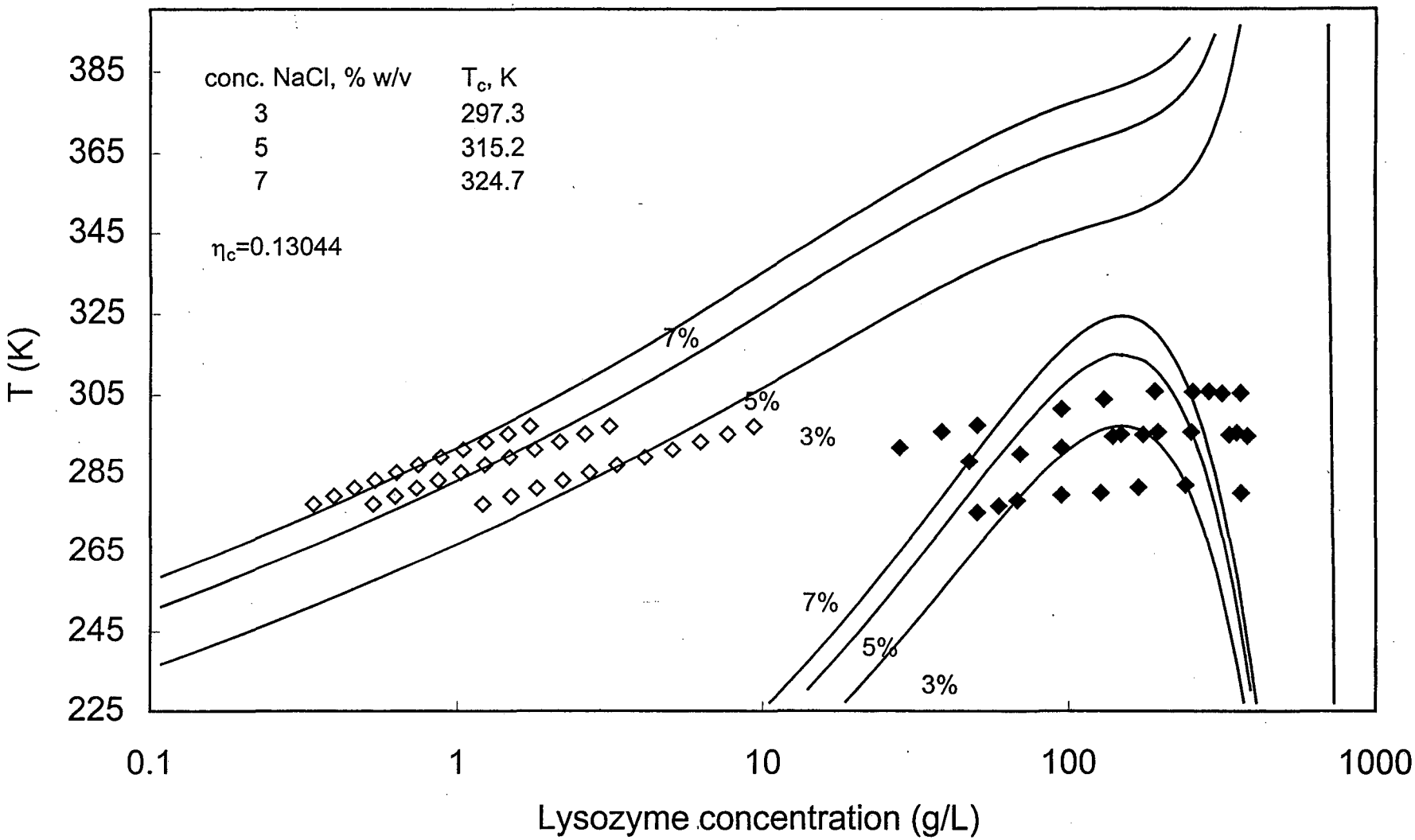
conc. NaCl, % w/v
T_c, K
3
297.3
5
315.2
7
324.7
η_c=0.13044
7%
5%
3%
7%
5%
3%
T (K)
385
365
345
325
305
285
265
245
225
0.1
1
10
100
1000
Lysozyme concentration (g/L)

Figure 3.a

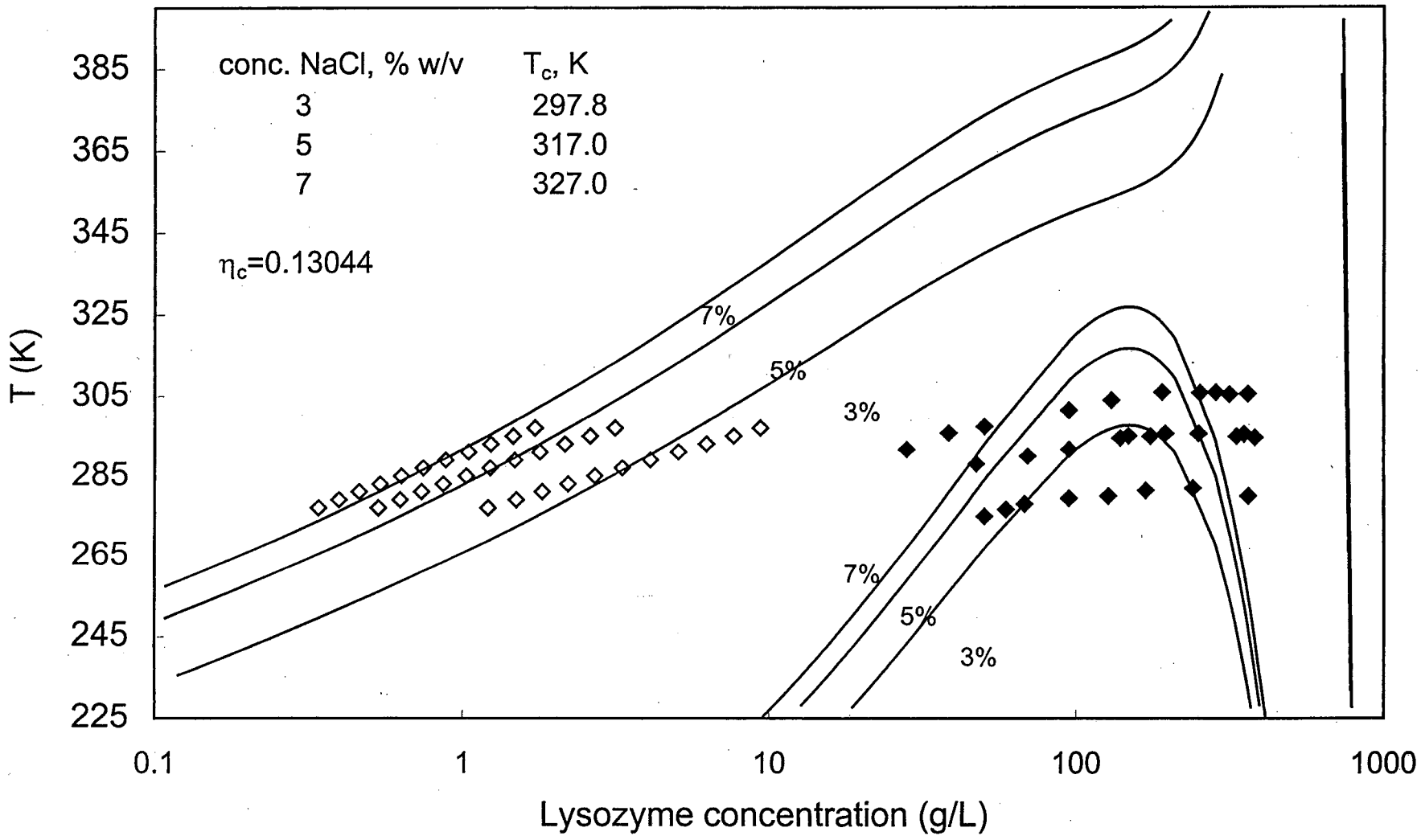
conc. NaCl, % w/v
T_c, K
3
297.8
5
317.0
7
327.0
η_c=0.13044
7%
5%
3%
7%
5%
3%
385
365
345
325
305
285
265
245
225
T (K)
0.1
1
10
100
1000
Lysozyme concentration (g/L)

Figure 3.b

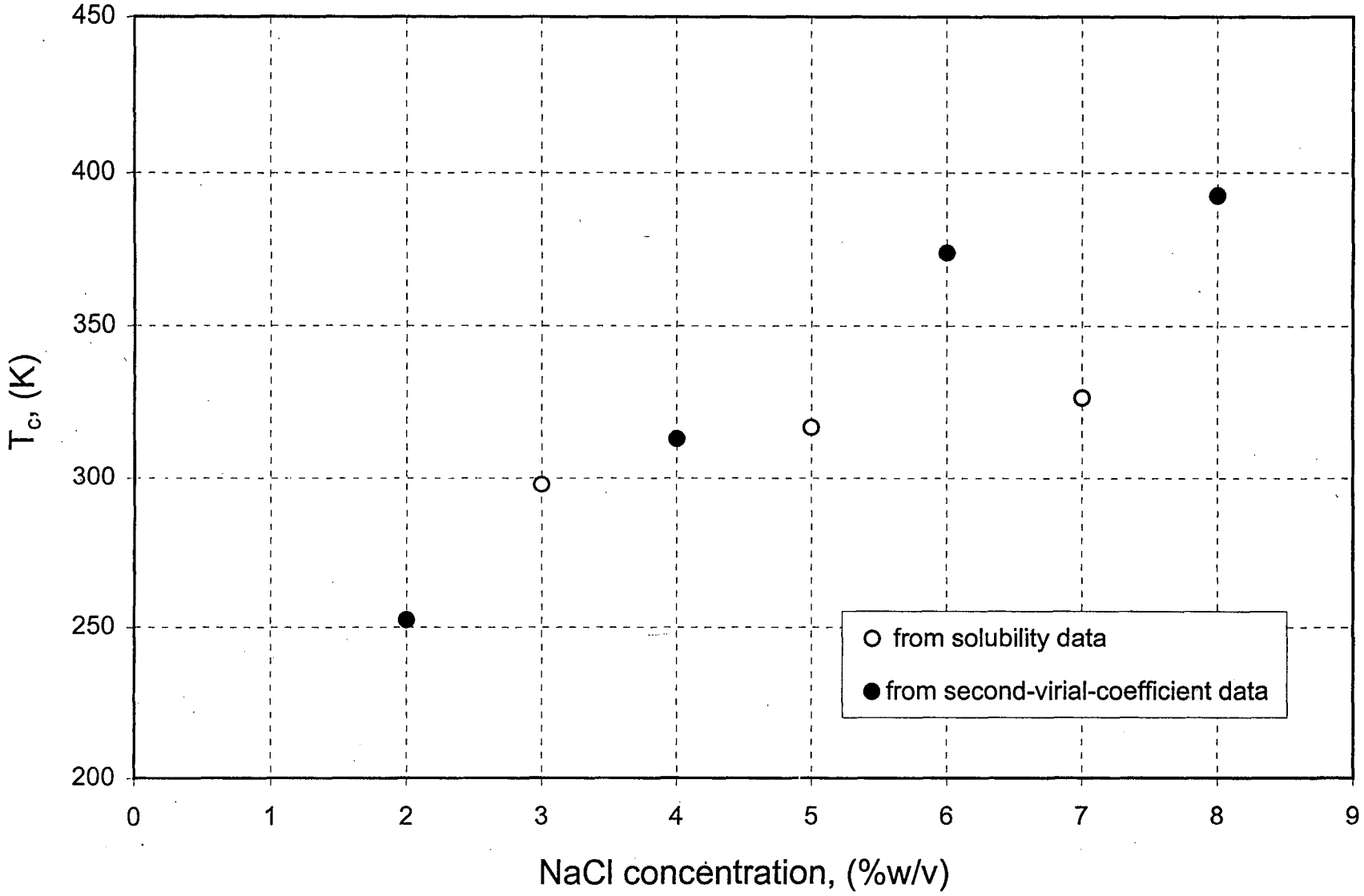
450
400
350
300
250
200
T_C, (K)
0
1
2
3
4
5
6
7
8
9
NaCl concentration, (%w/v)
from solubility data
from second-virial-coefficient data

Figure 4

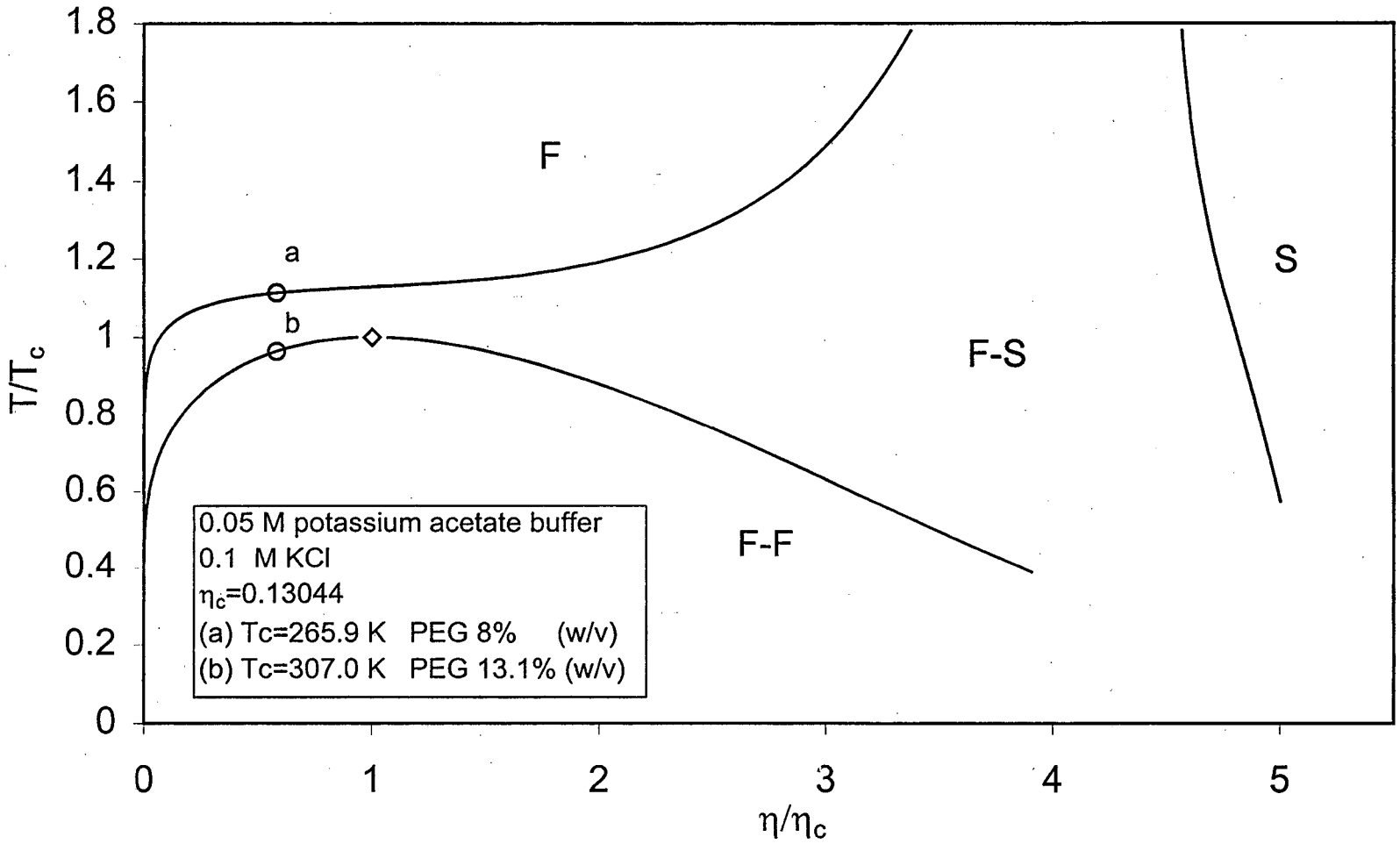
1.8
1.6
1.4
1.2
1
0.8
0.6
0.4
0.2
0
T/Tc
0
1
2
3
4
5
η/ηc
F
a
b
S
F-S
F-F
0.05 M potassium acetate buffer
0.1 M KCl
ηc=0.13044
(a) Tc=265.9 K PEG 8% (w/v)
(b) Tc=307.0 K PEG 13.1% (w/v)

Figure 5

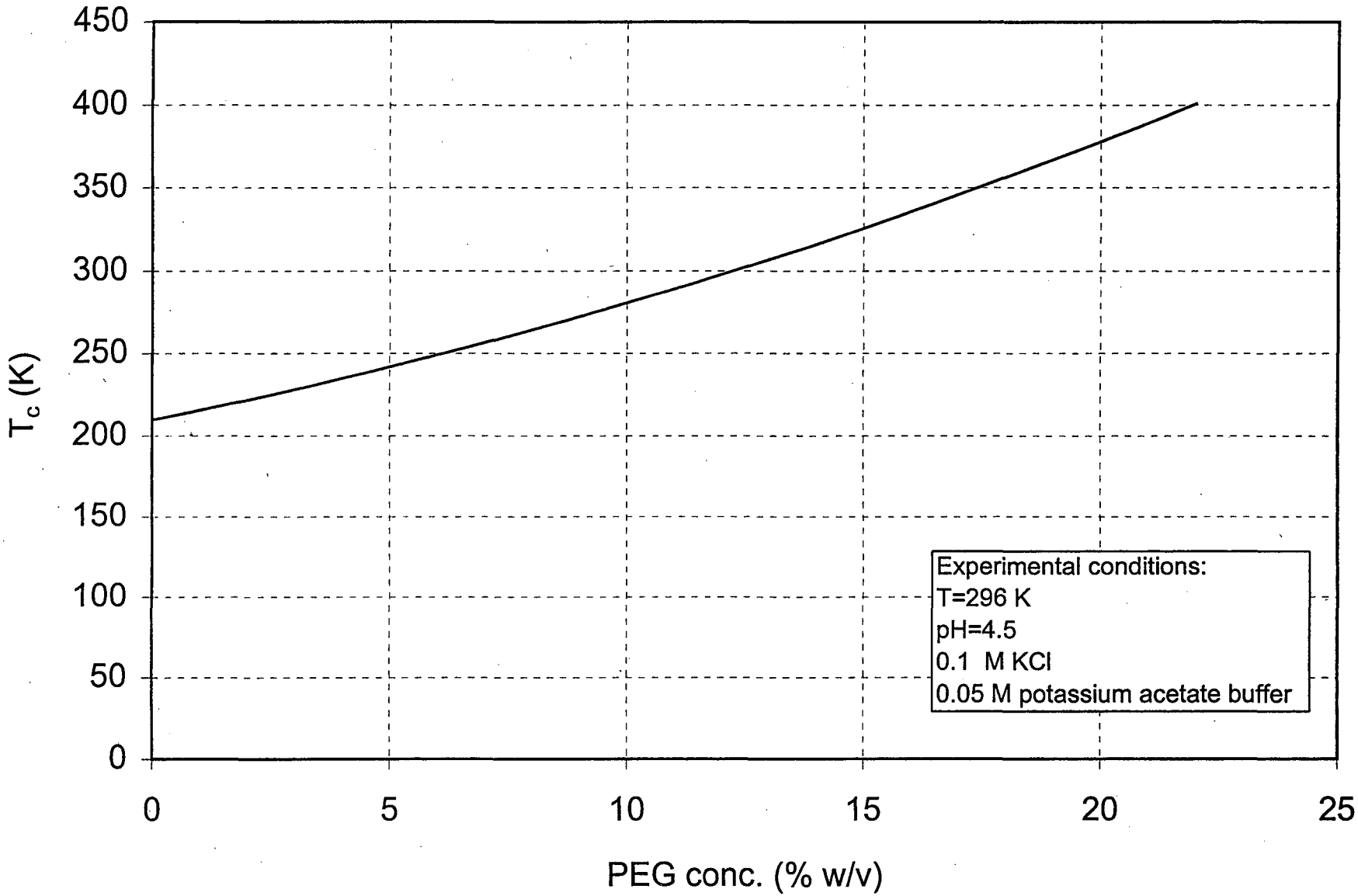
450
400
350
300
250
200
150
100
50
0
T_c (K)
0
5
10
15
20
25
PEG conc. (% w/v)
Experimental conditions:
T=296 K
pH=4.5
0.1 M KCl
0.05 M potassium acetate buffer

Figure 6

ERNEST ORLANDO LAWRENCE BERKELEY NATIONAL LABORATORY
ONE CYCLOTRON ROAD | BERKELEY, CALIFORNIA 94720

Prepared for the U.S. Department of Energy under Contract No. DE-AC03-76SF00098